ACS OMEGA

http://pubs.acs.org/journal/acsodf

Article

Binding of Per- and Polyfluoro-alkyl Substances to Peroxisome Proliferator-Activated Receptor Gamma

Nuno M. S. Almeida, Yiğitcan Eken, and Angela K. Wilson*

Cite This: *ACS Omega* 2021, 6, 15103−15114

Read Online

ACCESS | Metrics & More | Article Recommendations | Supporting Information

ABSTRACT: Peroxisome proliferator receptor gamma (PPARγ), a type II nuclear receptor, fundamental in the regulation of genes, glucose metabolism, and insulin sensitization has been shown to be impacted by per- and poly-fluoroalkyl substances (PFASs). To consider the influence of PFASs upon PPARγ, the molecular interactions of 27 PFASs have been investigated. Two binding sites have been identified on the PPARγ homodimer structure: the dimer pocket and the ligand binding pocket, the former has never been studied prior. Molecular dynamics calculations were performed to gain insights about PFASs-PPARγ binding and the role of acidic and basic residues. The electrostatic interactions for acidic and basic residues far from the binding site were probed, together with their effect on PPARγ recognition. Short-range electrostatic and van der Waals interactions with nearby residues and their influence on binding energies were investigated. As the negative effects of perfluorooctane sulfonate acid were previously shown to be alleviated by one of its natural ligands, L-carnitine, here, the utility of L-carnitine as a possible inhibitor for other PFASs has been considered. A comparison of the binding patterns of L-carnitine and PFASs provides insights toward mitigation strategies for PFASs.

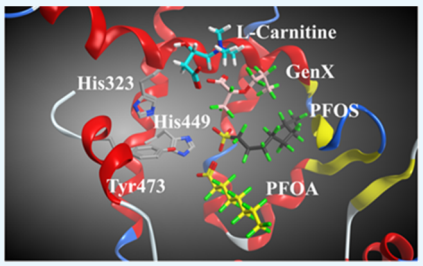

1. INTRODUCTION

Per- and poly-fluoroalkyl substances (PFASs) are "forever chemicals", a number of which have been implicated with long lasting effects on humans, animals, and the environment.[1] The first report of PFASs dates back to 1940.[2] Due to their oil- and fat-repellent properties along with their resilient nature, these chemicals were initially used for military purposes. Later, they were applied to industrial products, such as coating agents, oil repellents, and firefighting foam.[3−5]

Perfluorooctane sulfonate acid (PFOS) and perfluorooctanoic acid (PFOA) are the two most well-known PFASs. PFOA was initially used in commercial products to produce polytetrafluoroethylene, for non-stick coatings.[3] Several studies in the 1990s confirmed the presence of PFOS in blood serum. Eight chemical companies agreed to stop the production of PFOA and PFOS in 2006.[6] In 2015, the production of PFOS, PFOA, perfluorosulfonic acids with six or more carbon atoms, and perfluorocarboxylic acids with eight or more carbon atoms in the United States ended.[6,7] Despite safety concerns, which has stopped U.S. production and use, the manufacturing of these chemicals has continued in some countries.[8]

Recently, concerns have been raised about the possible levels of PFAS compounds in water sources, and mitigation efforts are underway in many states.[9] In 2016, the EPA released a health advisory recommending that the combined concentration of PFOS and PFOA in water should be less than 70 ng/L.[10] Despite the health advisory, there are no mandatory federal standards, and each U.S. state has its own regulations or guidelines for the safety of drinking water, ranging from 11 to 1000 ng/L.[10]

Assessing the impact of PFASs on organisms at the molecular level is fundamental to understand their possible effects and identify routes to mitigate them. The hepatotoxicity, neurotoxicity, reproductive toxicity, immunotoxicity, thyroid disruption, and cardiovascular toxicity of PFOS has been discussed by Zeng et al.[11] For a number of affected proteins linked to such toxicological impacts, there is crystal structure data available, facilitating molecular level studies. In addition, recent *in vivo* and *in vitro* studies have been conducted to study the interactions between human and animal proteins with PFASs (see, *e.g.*, refs 12−26).

In recent studies, PFOS was implicated in renal fibrosis.[27,28] The mechanism by which PFOS can cause renal injury involves the deacetylation and inactivation of PPARγ, playing a very important role in cell signaling processes. Liu et al. studied the associations of different PFASs and serum biochemical markers for uremic patients under hemodialysis.[29] They found that the effects of PFOS and PFOA on the kidneys are long-lasting and provided an explanation for the long half-life that PFASs have in humans.

PPARγ functions as a regulator for fatty acid storage and glucose metabolism by binding to DNA and acting as a

Received: March 10, 2021
Accepted: May 21, 2021
Published: June 4, 2021

transcription factor. The homodimerization of PPARγ and its biological relevance have been discussed in the literature.[30−35] Fulton et al. provides direct evidence that PPARγ homodimerizes by using yeast two-hybrid experiments, where the physical interaction between the two PPARγ monomers, and formation of homodimers, has been shown by reporter activation.[30] Todorov et al. studied nuclear receptor proteins from CaLu-6 cells probed with the ^{33}P-labeled human renin Pal3 sequence using electrophoretic mobility-shift assay.[31] The addition of anti-PPARγ antibody in these assays resulted in retardation of two separate protein complex bands. In other words, the anti-PPARγ antibody bound and slowed down two different PPARγ containing protein complexes present in the cells. Since RXRα is the standard interaction partner for PPARγ, Todorov et al. suggested that these two bands might correspond to the PPARγ/RXRα heterodimer and PPARγ/PPARγ homodimer.[31] Estany et al. found two inverted half site DNA motifs which may allow two PPARγ proteins to bind to each half site as a homodimer.[32] Okuno et al. utilized gel shift analysis showing that PPARγ might bind to the Pal3 DNA motif as a homodimer, in comparison to the DR1 motif, which is a commonly known PPARγ/RXR heterodimer binding site.[33] Many PPARγ crystals structures including the one reported by Nolte et al. and the one studied here (PDB ID: 3ADV) by Waku et al. show that PPARγ has a homodimer interface and can form a homodimer complex similar to other nuclear receptors (*i.e.*, estrogen receptor-α and RXR-α).[34,35] Due to the possible biological relevance of the PPARγ homodimer, the homodimer was considered in this study.

The activation of PPARγ causes insulin sensitization and regulates glucose metabolism, and the intake of any kinds of sugar is a fundamental process for the body to regulate. Chou et al. investigated how L-carnitine plays an essential role in attenuating the effects of PFOS in the kidneys *via* PPARγ and Sirt1 mechanisms.[27] Additionally, L-carnitine can be synthetized on a cellular level by methionine and lysine, and in prior studies, it is shown to diminish the effects of gentamicin-induced apoptosis in PPARα.[27,28]

To better understand PFAS structure/protein activity relationships, computational studies are important, although they are scarce. One of the first such studies was performed by Salvalaglio et al.[36] They examined the binding energies and binding sites in human serum albumin, describing how PFOS and PFOA bind to this protein. The authors utilized molecular dynamics simulations along with molecular mechanics-generalized Born solvation area (MM-GBSA) calculations to predict free binding energies[36] and described guidelines for PFASs with lower bio-accumulative potential. Other studies have utilized computation to investigate the interaction of different PFASs with human or animal proteins and analyze possible binding sites and poses.[37−40]

Takacs and Abbott investigated the interaction between PPARγ and PFOS and PFOA.[12] They observed that there was no PPARγ activity alteration in both mice and humans in the presence of these PFASs. Zhang et al. determined half maximum inhibition concentrations (IC_{50}) for twelve PFASs with PPARγ, providing docking and activity studies, and concluded that hydrogen bonding of the ligands to Tyr 473 and interactions with His 323 and His 449 were deemed essential for PPARγ activation. Additionally, the authors identified key residues and important hydrogen bond pairs on PPARγ for the ligand binding pocket (LBP) using molecular docking.[17] For PPARγ, different studies identify His 323, His 499, and Tyr 473 as key for PPARγ's activity, along with the size and length of the carbon chain (see example refs 41 and 42). In terms of structural properties, the importance of helixes AF-2, 3, 7, and 10 has been documented prior for PPARγ. The position of PFASs within the LBP and AF-2 helix, along with key residue interactions, is of paramount importance for PPARγ's activity.[17,43]

Activity and docking studies were also performed on PPARβ/δ using a range of PFASs by Li et al.[44] The authors found that the binding geometries of selected PFASs were similar to those of fatty acids, fitting in the LBP of PPARβ/δ. Furthermore, Li et al. found that both isoforms of PPAR are activated by PFASs, and that the transcriptional activity was associated with the carbon length.[44] Recently, Behr et al. probed the activation of nuclear receptors with PFAS.[18] Although PPARα could activate several PFASs, PPARγ was shown to only be activated by perfluoro-2-methyl-3-oxahexanoic acid and 3*H*-perfluoro-3-[(3-methoxypropoxy) propanoic acid. In comparison with *in vitro* experimental results by Zhang et al., Behr et al. reported much different PPARγ activity. These inconsistencies were attributed to the PPARγ constructs selected, and different cell lines were used in the experiment.[17,18] Due to the conflicting conclusions from the prior studies, a better understanding of how PPARγ interacts with different residues at a molecular level is needed.

In this study, different binding pockets are investigated, as well as the interactions between PPARγ and 27 widely used PFASs. Herein, in addition to the orthosteric binding pocket present in the PPARγ LBD, a new binding site present in the PPARγ homodimer is identified: dimer pocket and studied as a potential bio accumulative target. The dimer pocket is situated between the two PPARγ LBD monomers, and computational predictions showed binding to a variety of PFASs.

The PFASs investigated here represent a variety of carbon chain lengths and functional groups (amines, carboxylic groups, alcohols, and sulfonic groups) to provide insights about how structural modifications affect the binding of PFAS species to the receptor. A number of "short chain" PFAS alternatives are considered including 2,3,3,3-tetrafluoro-2-heptafluoropropoxy propanoic acid (GenX), 4,8-dioxa-3H-perfluorononanoic acid (ADONA), 6:2 fluorotelomer carboxylic acid (6:2 FTCA), and 6:2 fluorotelomer alcohol (6:2 FTOH). "Short chain" alternatives to PFOS and PFOA are perfluoroalkyl carboxylic acids (PFCAs) with six or less fluorinated carbons and perfluorosulfonic acids (PFSAs) with five or less fluorinated carbons. "Short chain" PFASs are generally thought to be less harmful; however, their effects on the human body and environment are less understood.[45−47] The influence of basic and acidic residues upon the interactions has been investigated, as has the impact of L-carnitine and its interaction with different binding pockets.

2. COMPUTATIONAL METHODS

2.1. Site Analysis and Molecular Docking. The PPARγ dimer structure was taken from the RSCB Protein Data Bank (PDB ID: 3ADV[35]) and was protonated using the Protonate 3D[48] program from the Molecular Operating Environment's (MOE).[49] 3ADV structure is a PPARγ homodimer, which has seen less attention in the literature and allowed us to identify a new binding site for PFASs (dimer pocket). Additionally, 3ADV has a fatty acid metabolite, which has an amphiphilic nature similar to PFASs and also has good X-ray resolution (2.27 Å), which allows for detecting positions of the side chain

https://doi.org/10.1021/acsomega.1c01304
ACS Omega 2021, 6, 15103−15114

atoms confidently.[35] The protonated PPARγ dimer was scanned for potential binding pockets using MOE's "site finder". The site finder program detects alpha shapes on the protein surface and evaluates them according to their propensity of ligand binding (PLB) score.[50]

The initial structures of the PFASs and L-carnitine were obtained from PubChem.[51] The chemical formulas and acronyms for the PFASs can be found on Table S1, and the chemical structures of the compounds are included in Table S2. The protonation states of the PFASs and L-carnitine under physiological conditions (pH 7, 300 K and 1 atm) were determined using the Protonate3D module and were minimized in MOE with the AMBER10: Extended Hückel Theory (EHT) force field, which uses Amber ff10 for macromolecules and EHT for the ligands.[52−54] PFASs' and L-carnitine's binding modes to the dimer pocket and LBP were determined by docking to the binding sites using MOE.[49] During the generation of L-carnitine binding poses to the LBP, the hydrogen bond to the Tyr 473 was implemented as a query for a pharmacophore approach, which is associated with PPARγ activity.

The London ΔG scoring function was used to evaluate 100 initial ligand placements.[55] Then, these initial 100 placements were further refined to ten poses *via* the generalized-born volume integral/weighted surface area scoring function (GBVI/WSA) ΔG with induced fit protein settings. The structurally distinct refined poses with the highest (GBVI/WSA) ΔG scores were selected for further studies.

2.2. Simulation Protocol. The selected complex structures were minimized using molecular mechanics (MM) with the Amber10:EHT forcefield in MOE.[52−54] The topologies and the parameters for the minimized structures were created using the Leap module of Amber Tools[56] by using general amber force field (GAFF) and AMBER ff14sb force fields.[57] The AM1-BCC charge scheme[58] was used to calculate partial charges of the ligand atoms, and these partial charges were fit to GAFF by using the antechamber[56] suite to generate ligand parameters. The protein−ligand complex structures were placed in a 14 Å cube beyond the solute box, neutralized, and ionized with 100 mM NaCl ions using parameters from Joung and Cheatham in order to replicate a biological ionic environment.[59]

In the minimization protocol, a series of harmonic potentials (500.0, 200.0, 20.0, 10.0, 5.0, and 0.0 kcal mol^{-1}) were used, which restrain the protein structure and allow water molecules, ions, and the ligand to relax. Then, the systems were heated from 100 to 300 K in 30 ps MD simulations. After heating, 30 ns MD simulations were performed to ensure the convergence of the system at 300 K and 1 atm pressure (see example rmsd plots in Supporting Information, Figures S8−S11). During all simulations, the pressure and temperature were controlled by isotropic position scaling and Langevin dynamics, respectively. Furthermore, the SHAKE algorithm[60] was used to constrain hydrogen bonds which allowed the use of a 2 fs time step. Non-bonded interactions were truncated to 10 Å, while the particle-mesh Ewald method was used to efficiently approximate long-range electrostatic interactions. The minimization protocol and MD simulations were performed with Amber.[56]

2.3. Binding Energy Calculations. The binding free energies of the ligand−protein complexes were calculated using both molecular mechanics Poisson−Boltzmann surface area (MM-PBSA) and MM-GBSA with a modified general born solvation model[61] implemented in the Amber PBSA-solver.[62] The default internal and external dielectric constants were used (1.0 and 80.0, respectively). The solvent accessible surface area was determined with the default linear combinations of pairwise overlaps method using modified Bondi atomic radii. Due to the high computational cost of the methodology, 500 frames of the simulation were used for the MM-GBSA and MM-PBSA calculations. As shown in Figures S8−S11, the overall protein rmsd has reached stability by this point, so longer simulations are not necessary. A prior paper has demonstrated that choice of different/longer time frames will have little impact on the binding energy predictions.[63] The solute entropies were not considered because the primary focus of this effort was on the relative binding energies of the ligands on PPARγ. The binding contributions of the residues were calculated by per-residue decomposition,[56] and the energy contribution for each acidic and basic residues were averaged from all of the poses tested. The residue decomposition was performed using CPPTRAJ from Amber, and the full length of the simulation was considered.[56,64] This step is important to understand specific interactions, selectivity, and recognition in PPARγ.

2.4. Hydrogen Bonding Analysis. Hydrogen bond lifetime analyses were performed *via* CPPTRAJ for every ligand tested.[64] The ligand-PPARγ complex with the strongest MM-PBSA relative binding energy was selected for analysis.

3. RESULTS AND DISCUSSION

3.1. Binding Pockets on PPARγ. The two potential binding sites with the highest PLB scores, referred to here as the dimer pocket and the LBP, were investigated and are shown in Figure 1. The dimer pocket, not previously studied, has the highest PLB score in comparison to other pockets. It is located between the two PPARγ dimer structures and is ∼1900 $Å^3$ in size. This is in contrast to the LBP, which is ∼1300 $Å^3$ in size. The LBP is known to bind to a variety of ligands (*i.e.*, medium chain fatty acids, thiazolidinediones, phenyl acetic acids, and phenyl propanoic acids).[65−67] In this study, both the

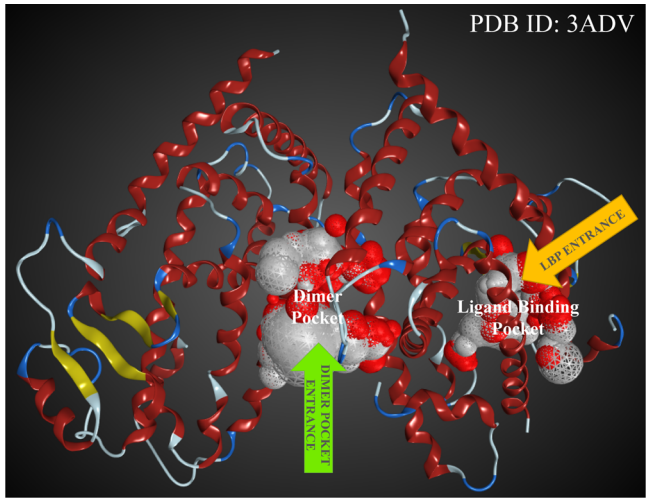

Figure 1. Binding pockets detected on the PPARγ dimer structure (PDB ID: 3ADV) using MOE's Site Finder. Two potential binding sites are identified, and their entrances are shown. The surface and area of the binding sites are depicted. The red spheres indicate a hydrophilic surface, while silver depicts hydrophobic surfaces.

https://doi.org/10.1021/acsomega.1c01304
ACS Omega 2021, 6, 15103−15114

dimer pocket and the LBP were considered as potential binding sites for the PFASs (Table S1) and L-carnitine.

3.2. Binding Poses of PFASs. To determine how PFASs orient within the potential binding sites, molecular docking was used. The ligand binding to PPARγ is a complex process. The PPARγ receptor contains flexible binding cavities and can host a variety of structurally distinct ligands.[68] Due to the complexity of binding, induced-fit docking is used during the pose generation. Induced-fit docking accounts for the movements in the protein structure upon ligand binding and multiple binding possess generated during this step are further evaluated through MD and binding free energy calculations. The binding poses with highest affinity are evaluated through the residue decomposition schemes and hydrogen bond analysis. The highest affinity binding poses of the ligands into the LBP and the dimer pocket are shown in Figures 2 and S1, respectively. PFASs which have more than six and less than 14 per-fluorinated carbon orient their functional groups toward Tyr 473, His 449, and His 323, which have previously been proposed as important residues for PPARγ activity.[17]

3.3. Binding Free Energy Calculations (MM-GBSA/MM-PBSA) and Correlation Plots. The binding modes of PFASs and L-carnitine to the LBP and dimer pocket were studied using MM-GBSA and MM-PBSA, and the resulting binding energies are depicted in Figures 3 and S2, respectively. The binding energies were determined by averaging the results for different PPARγ binding poses for each compound. In comparing the experimental IC_{50} values by Zhang et al. (see, ref 17) to our predicted PFASs to LBP binding energies, better correlation was obtained using MM-PBSA rather than MM-GBSA.

The binding energy values correlate directly with the carbon chain length; however, the effects of the carbon chain length differ for the dimer pocket and the LBP. On average, the binding energies for the dimer pocket were lower than for the LBP. Et-PFOSA-AcOH and Me-PFOSA-AcOH showed high affinity toward the dimer pocket. Their chain lengths in addition to their sulfonic and carboxylic functional groups enabled very strong interactions (~25 kcal mol^{-1}). L-Carnitine also showed strong binding to the dimer pocket and strong residue interactions (see Section 3.4).

The PFASs showed stronger binding to the LBP than to the dimer pocket, while L-carnitine showed similar binding to both pockets according to MM-PBSA. This indicates that PFASs are prone to bind more strongly to the LBP, although the dimer pocket can still have a role on the accumulation of PFASs. Ligand binding to LBP is important for the activity of PPARγ (see, *e.g.*, ref 17). In order to assess how the calculated binding energies for LBP correlate to the PPARγ activity, IC_{50} values of PFDA, PFNA, PFHxS, PFOA, PFOS, PFHxDA, PFOcDa, PFTeDA, and PFDoA determined by Zhang et al. are used for comparison, as shown in Figure 4. The binding energies of PFOcDA and PFHxS were calculated only for the LBP to compare with respective experimental IC_{50} values by Zhang et al.[17] The predicted binding energies of L-carnitine show that it can compete to replace PFASs from both binding sites.

On average, the affinity of PFASs to LBP increased with the size of the carbon chain length. There is a rise in binding energy from PFBA to PFOcDA, which is consistent with the increasing size of the carbon chain length. The LBP is approximately three times larger than other nuclear receptors' ligand pockets, which allows for compounds as large as PFOcDA to bind strongly.[65] PFASs with sulfonic acid groups

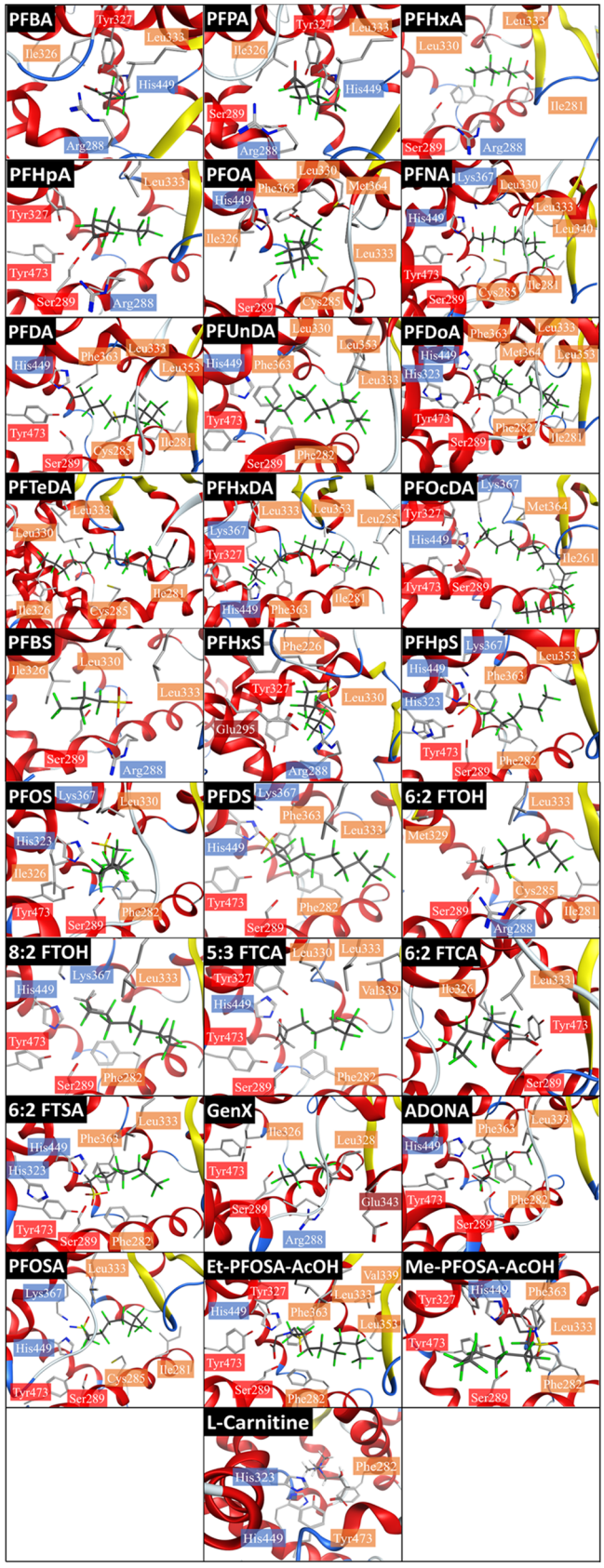

Figure 2. Binding poses of PFASs and L-carnitine on PPARγ. The binding modes that have the highest binding affinity determined from MM-PBSA are shown. Residues depicted belong to chain A.

https://doi.org/10.1021/acsomega.1c01304
ACS Omega 2021, 6, 15103−15114

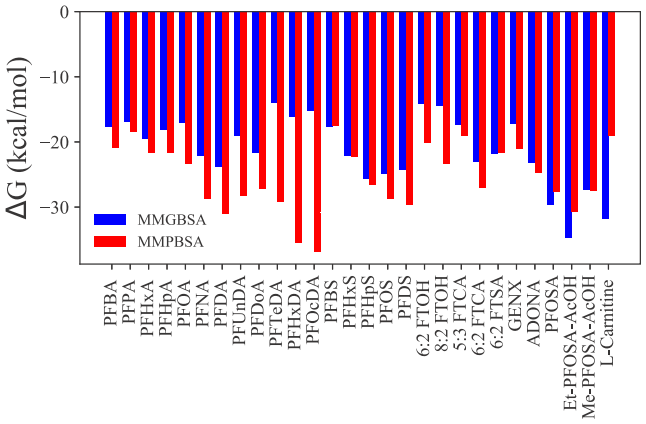

Figure 3. Average binding energies of PFASs and L-carnitine calculated with MM-GBSA and MM-PBSA for the LBP. PFASs are divided into subgroups: PFCAs, followed by perfluoroalkyl sulfonic acids (PFSAs), fluorotelomer alcohols (FTOHs), fluorotelomer carboxylic acids (FTCAs), fluorotelomer sulfonic acids (FTSAs), and then alternatives. Each subgroup was listed from the shortest chain length to longest (see Supporting Information Tables S1 and S2 for acronyms and structures).

showed higher affinity to the LBP in comparison to the carboxylic acids, fluoro telomer alcohols (FTOHs), and fluoro telomer carboxylic acids (FTCAs), with the same number of per-fluorinated carbons. The PFASs that have a six to eight per-fluorinated carbons along with both sulfonic acid and carboxylic acid groups (Et-PFOSA-AcOH and Me-PFOSA-AcOH) showed strong binding to LBP and to the dimer pocket.

In recent work, MM-GBSA and MM-PBSA binding energy predictions were evaluated for PFASs and the hPXR protein.[69] In this prior study, both MM-PBSA and MM-GBSA correlate well with the experimental EC_{50}, though the MM-GBSA correlation was slightly better.[69] However, large PFAS molecules such as PFTeDA, PFHxDA, and PFOcDA were not studied for the hPXR receptor, and for these larger molecules, MM-GBSA and MM-PBSA differ. As shown previously, the utility of MM-GBSA and MM-PBSA can vary with respect to the studied system.[70] Factors such as hydrophobicity, lipophilicity, and electrostatics of the ligand and choice of binding site, all play an important role on the performance of the theoretical methods, directly influencing computed predictions. For the large PFASs (PFTeDA, PFHxDA, and PFOcDA), the tail portion of the compound is more solvent-exposed and MM-PBSA provides a more rigorous treatment of these solvent effects; thus, MM-PBSA results in better correlation with experimental IC_{50} values. For this reason, only the MM-PBSA correlation plot (Figure 4) has been included. The MM-GBSA correlation is shown in Figure S3. The r^2 between calculated binding energies and experimental IC_{50} values is 0.6, which indicates that the calculated binding energies for LBP correlate with the activity data, although some variance is observed. This variance is associated with both experimental and calculated standard deviations. Another element that contributes to lower correlation is the fact that experimental IC_{50} values relate to the structure activity data, which is not the case for MM-GBSA or MM-PBSA. For example, for 6:2 FTOH or 8:2 FTOH, Zhang et al. does not detect any activity experimentally; however, in the current study, these species do bind, though they do not contribute to the receptor's activity. PFHpA is an outlier and has not been included in Figure 4, due to its large IC_{50} value and large experimental uncertainty for PPARγ activation (192.4 ± 17.2).

3.4. Residue Decomposition Analysis. *3.4.1. Binding Contribution from Nearby Residues to PFASs and L-Carnitine.* To evaluate the contribution of nearby residues to the Gibbs free energy of binding, a space of 5−6 Å around PFASs and L-carnitine was selected. The binding energy contribution within this space was determined *via* a per-residue decomposition, which accounts for electrostatic and van der Waals contributions to the binding. The average residue contributions for PFASs (red) and L-carnitine (green) were determined from the highest affinity poses for the LBP and dimer pocket and are compared in Figures 5 and S5, respectively. At pH 7, L-carnitine is neutral, but it has two charged groups. One side of the molecule is positively charged ($N^+C_3H_9$), and the other side has a deprotonated carboxylic

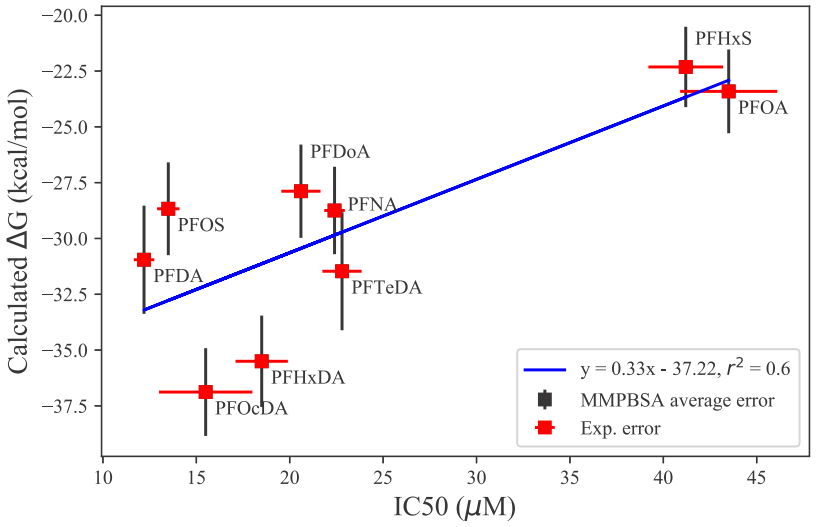

Figure 4. Average calculated binding energies of PFASs with MM-PBSA in comparison with IC_{50} values determined experimentally by Zhang et al. On the *y*-axis, the average calculated binding energies are plotted, and along the *x*-axis, the experimental IC_{50} values are provided. Error bars are depicted in black (MM-PBSA) and red (experimental).

https://doi.org/10.1021/acsomega.1c01304
ACS Omega 2021, 6, 15103−15114

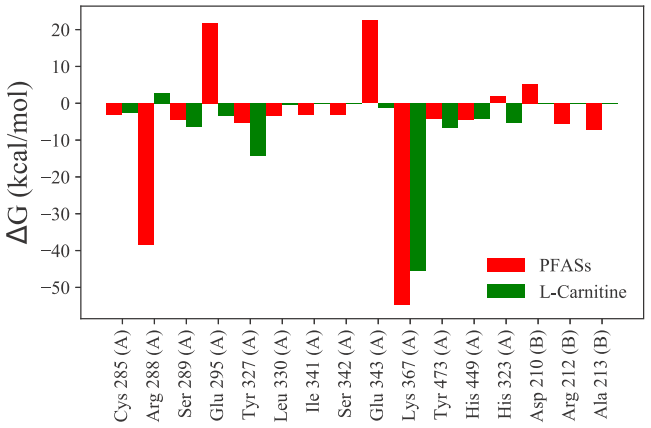

Figure 5. Binding contribution of each nearby residue for PFASs and L-carnitine (LBP). For PFASs, highest affinity poses are averaged, and for L-carnitine, the highest affinity pose is used.

group (COO^-). It also has an OH group which can serve as a hydrogen donor (Section 3.5). As discussed in Section 3.3, L-carnitine shows similar binding energies to the dimer pocket and LBP, with average binding energies of −19.0 kcal mol^{-1} from MMPBSA (Tables S3 and S4).

For the dimer pocket, the acidic residues such as Glu 324, Asp 396, Glu 407, and Asp 441 repel PFASs derivatives very strongly, as demonstrated by the average binding contributions of ∼30 kcal mol^{-1} (Figure S4). For L-carnitine, the acidic residues contribute positively or negatively to the overall energy depending on their orientation toward the NH_3^+ and COO^- groups in the molecule. For example, in the dimer pocket, L-carnitine is repelled by Glu 324 (15 kcal mol^{-1}), whereas Glu 407 has a negative contribution to the binding energy (−15 kcal mol^{-1}). The interaction energy of L-carnitine with basic residues especially arginines and lysines is significant, but not as strong as for PFASs.

Figure 5 shows the interaction energy of PFASs with close residues within the LBP. As shown, Arg 288 and Lys 367 have the strongest contributions to the binding, whereas Glu 295 and Glu 343 repel PFASs from binding to the LBP. In contrast, L-carnitine is not repelled by Glu 295 and Glu 343 and additionally showed strong interaction energy with Lys 367. Tyr 473 contributes slightly to the binding of PFASs and L-carnitine to the LBP, due to the hydrogen bonding observed with the long carbon chain molecules. (Zhang et al. proposed hydrogen bonding to Tyr 473 as key to the PPARγ activity.[17] The hydrogen bonding interaction is discussed in Section 3.5). L-Carnitine has a −6.6 kcal mol^{-1} interaction energy to Tyr 473, compared to a slightly lower value of average PFASs. PFASs that are shorter in length such as PFBA and PFPA did not form a hydrogen bond with Tyr 473 (Figure 8).

As the importance of His 449 and His 323 PPARγ activity has been reported,[41,65] the role of these residues is examined. His 449 has an interaction energy of ∼−5 kcal mol^{-1}, with the PFASs and L-carnitine. For His 323, the calculated interaction energy was −5.3 kcal mol^{-1} for L-carnitine, but positive for PFASs.

3.4.2. Binding Energy Contribution from Acidic and Basic Residues to PFASs and L-Carnitine. A residue decomposition of PPARγ in terms of long-range electrostatic interaction was done. To date, there is no such study done for PPAR receptors. Here, we consider two questions: how are ligands affected by long-range interactions? How is the LBP affected by residues on the other side of the protein?

To investigate these questions, basic residues (arginines, lysines, and histidines) and acidic (glutamate and aspartate) residues within the PPARγ dimer were studied from the A and B chains. All ligand poses were considered for the dimer pocket and LBP. Average interaction energies for all of the PFASs investigated were compared with the L-carnitine interaction energy. In Figures 6 and 7, the average interaction energies for LBP are shown for PFASs and L-carnitine, respectively.

The average interaction energies for the dimer pocket can be found on Figures S5 and S6. As the dimer pocket is situated between the two monomers (Figure 1), it is able to interact with both chains of the protein (almost symmetrically, when comparing the energies of chain A and chain B). For basic residues, the strongest interactions are observed with Arg 397, Arg 443, Lys 373, Lys 434, and Lys 438, and for acidic residues, the strongest repulsion is observed with Asp 396, Glu 324, Glu 407, and Asp 441 (>±25 kcal mol^{-1}). The short-range electrostatic interactions within the chains of the protein can stabilize the ligand or repel it. When comparing PFASs with L-carnitine, the average interaction energies for the PFASs with Asp 396, Glu 324, Glu 407, and Asp 441 reveal a different trend than for L-carnitine. PFASs are strongly repelled by these residues, while L-carnitine is only slightly repelled (∼5 kcal mol^{-1}) by Glu 324 but attracted by the other ones.

Considering the LBP, the strongest interactions correspond to residues in chain A (Arg 288, Lys 367, Glu 291, Glu 295, and Glu 343), which are situated mainly in the LBP (Figures 6 and 7). There are large contributions from the residues on the other chain that range from −5 to −15 kcal mol^{-1} for the basic residues and 5−15 kcal mol^{-1} for the acidic residues.

For L-carnitine, considering the acidic residues' interaction energy, there is a different trend compared to PFASs (Figure 7). The acidic residue energies vary from positive to negative, which shows that not all are repulsive toward L-carnitine. Regarding basic residues, Lys 367 is the major contributor toward its affinity in the pocket and contributes strongly to the LBP binding.

3.5. Hydrogen Bonding. A detailed analysis of the propensity of the dimer pocket and LBP to hydrogen bond is fundamental for understanding the intermolecular interactions between ligands and residues. By using MD trajectories, it is possible to understand fundamental binding properties and the activity of the receptor/protein. Herein, some of the ligands: 6:2 FTOH, 8:2 FTOH, L-carnitine, Et-PFOSA, and Met-PFOSA can be hydrogen donors or acceptors (Figures 8 and S7).

In Figure S7, the hydrogen bonding percentage is shown for the dimer pocket. Lys 438, Arg 443, and Arg 397 have the highest percentage of hydrogen bonding. These residues were noted earlier (Section 3.4.1) as being in close proximity to the ligands in the binding cavity. L-Carnitine is stabilized in this pocket by three hydrogen bonds with Gln 437, Arg 443, and Ser 394. L-Carnitine's positive and negative charged groups allow for different bonding with residues in the dimer pocket. Et-PFOSA-AcOH and Met-PFOSA-AcOH have very strong affinity to the dimer pocket and form strong hydrogen bonding with Arg 443. The sulfonic and carboxylic functional groups interact strongly with nearby residues. In addition, Et-PFOSA-AcOH and Met-PFOSA-AcOH are also stabilized by the interaction with Asp 396 and Gln 444. In the dimer pocket,

https://doi.org/10.1021/acsomega.1c01304
ACS Omega 2021, 6, 15103−15114

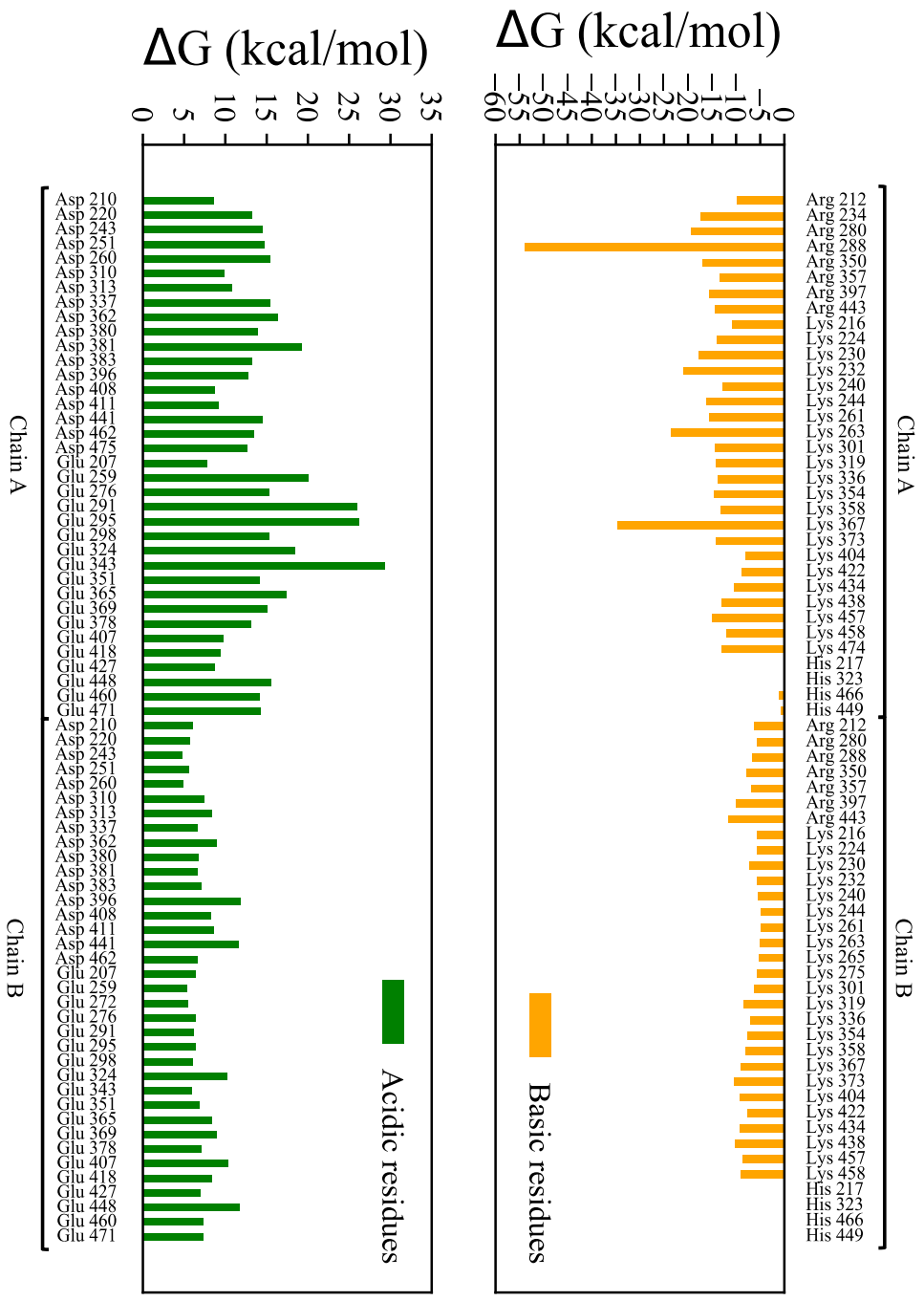

Figure 6. Binding contributions of the acidic and basic residues for PFASs (LBP) in chain A and chain B.

hydrogen bonding from fluorines can occur, though it is minimal.

In Figure 8, the LBP hydrogen bonding is described for PFASs and L-carnitine. As mentioned earlier, hydrogen bonding to Tyr 473 is directly associated to the activity of the receptor. PFASs with 7-12 perfluorinated carbons such as PFHpA, PFOA, PFNA, PFDA, PFDoA, PFOS, Et-PFOSA-AcOH, and Met-PFOSA-AcOH show high affinity to this residue. PFOS, Et-PFOSA-AcOH, Met-PFOSA-AcOH, and PFDS have a sulfonic group, which enables them to undergo strong hydrogen bonding, occurring for nearly the entire simulation. From the literature, 6:2 FTOH, 8:2 FTOH, 6:2 FTCA, PFBS, and PFBA show no activity, which is corroborated in Figure 8; there is no hydrogen bonding to Tyr 473.[17] Even though PFTeDA, PFHxDA, and PFOcDA show activity experimentally, the MD simulations do not show hydrogen bond formation with Tyr 473. There are examples of PPARγ agonists that do not form H-bonds with Tyr 473 but are still able to activate a receptor through immobilization of the H12 helix.[17,43] Due to the size of these larger PFASs, the binding poses obtained for them were more distant from Tyr 473 and more solvent-exposed, and thus, the hydrogen bonding with Tyr 473 is not demonstrated. Also, the scope of this study was to compare relative binding energies of various PFASs and understand the molecular interactions behind the PPARγ recognition. For this purpose, 30 ns MD simulations were performed, allowing more PFAS molecules and poses to be considered. PFASs alternatives such as

https://doi.org/10.1021/acsomega.1c01304
ACS Omega 2021, 6, 15103−15114

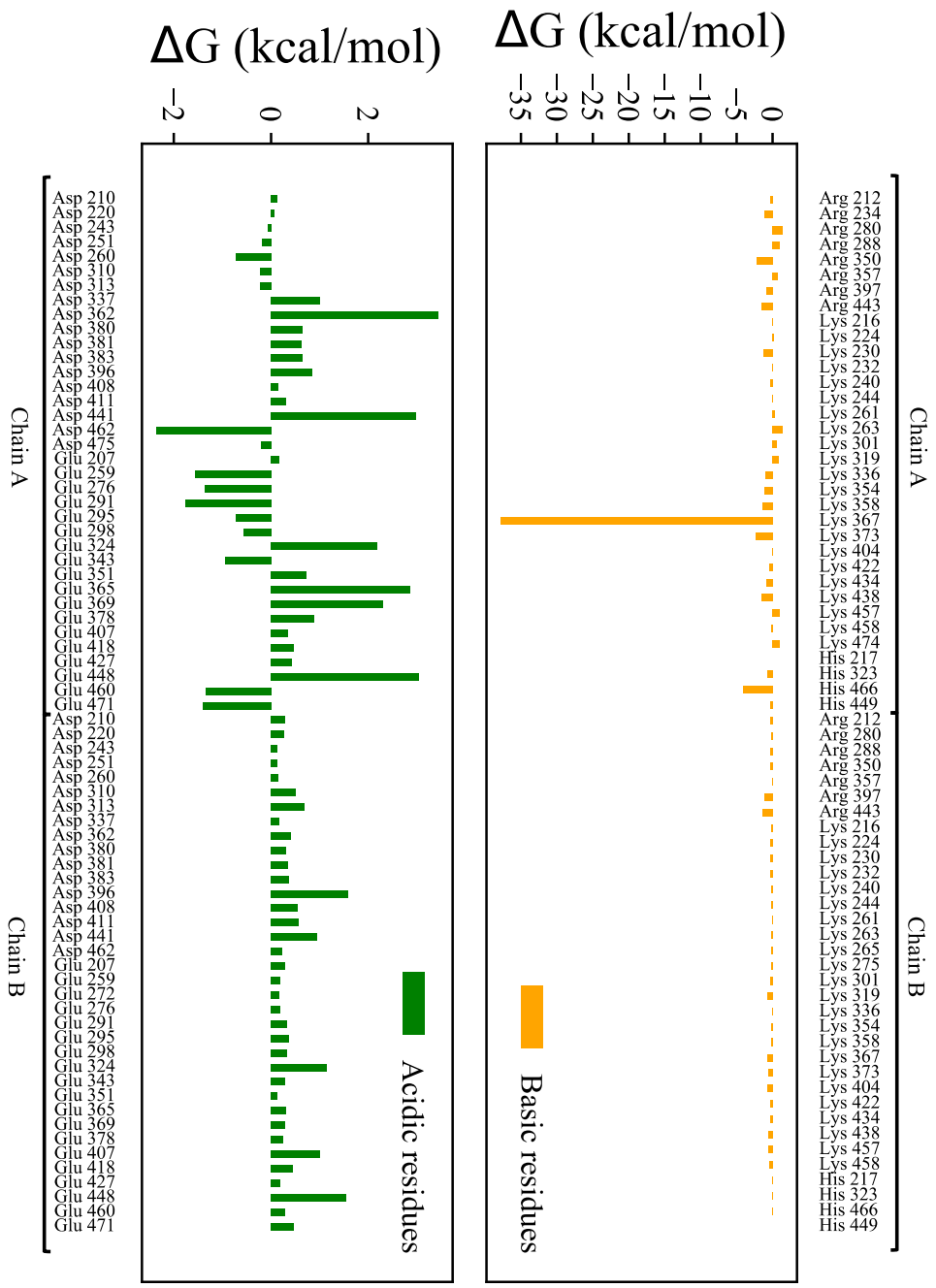

Figure 7. Binding contributions of the acidic and basic residues for L-carnitine (LBP) in chain A and chain B.

ADONA, GenX, 6:2 FTOH, 6:2 FTCA, Et-PFOSA-AcOH, and Met-PFOSA-AcOH have large binding energies, but not all of them showed hydrogen bonding with Tyr 473 during MD simulations. Short-chain PFASs exhibit binding toward PPARγ, yet they show limited hydrogen bonding with Tyr 473. PFASs that have between six and twelve carbons form strong hydrogen bonds with Tyr 473 and alter PPARγ's activity. L-Carnitine forms strong hydrogen bonds as an acceptor with Tyr 327, Lys 367, His 449, and Tyr 473 (Figure 8). As a donor, it also interacts with Ser 289. ADONA is a proposed alternative to PFASs and also forms a hydrogen bond with Tyr 473, which shows its ability to activate PPARγ. Tyr 327 and Lys 367 form a hydrogen bond with a range of PFASs.

4. CONCLUSIONS

The interactions of twenty-seven PFAS molecules and one of its natural ligands, L-carnitine with two potential binding pockets on the PPARγ dimer, were investigated. Possible poses for the PFASs and L-carnitine, their binding energies, and important residue interactions, including hydrogen bond analysis were evaluated. The role of the dimer pocket is discussed and shown to be important for binding PFASs and L-carnitine. The PFASs' binding energies predicted for the dimer pocket show evidence for potential bioaccumulation of PFASs at this site. Significant correlation is observed between the predicted binding energies for the LBP and experimental IC_{50} values of PFASs in PPARγ, which allowed the activity of the remaining PFASs to be estimated.

https://doi.org/10.1021/acsomega.1c01304
ACS Omega 2021, 6, 15103−15114

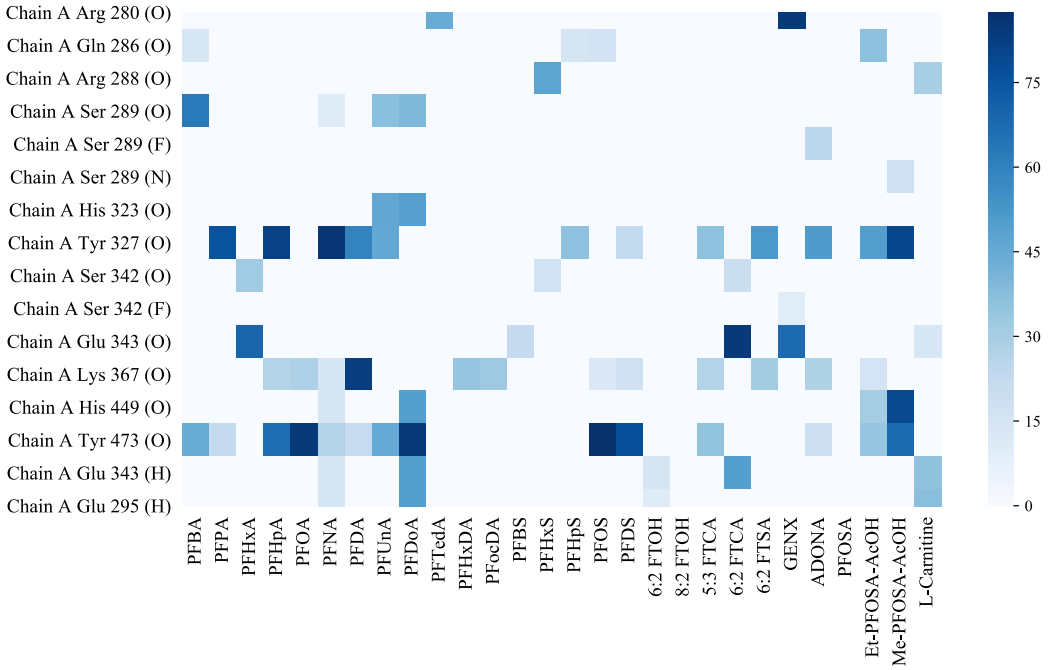

Figure 8. Hydrogen-bond lifetimes for the LBP. The *y*-axis depicts the chain and residue number from the receptor, and in brackets, the atom from the ligand performing the hydrogen bonding is shown. Acceptors are portrayed by "(O), (F), (N)", and donors by "(H)". In the *x*-axis, the different PFASs and L-carnitine are shown.

Shorter-chain PFASs, such as PFBA, PFPA, 6:2 FTCA, Met-PFOSA-AcOH, and Et-PFOSA-AcOH bind strongly to the dimer pocket, which indicates their potential bioaccumulation at this site. The PFASs in this study that have between six and twelve carbons form strong hydrogen bonds with Tyr 473 and may alter PPARγ's activity. PFAS alternatives such as ADONA, GENX, 6:2 FTOH, 6:2 FTCA, Et-PFOSA-AcOH, and Met-PFOSA-AcOH also have large binding energies, but not all of them showed hydrogen bonding with Tyr 473 during MD simulations, which is deemed essential for PPARγ activation. L-Carnitine also showed hydrogen bonding with Tyr 473.

The affinity of L-carnitine to LBP determined by MMPBSA is -19.0 kcal mol^{-1}, which shows similar binding in comparison to most of the PFASs. In addition, acid/base and short distance residue interactions contribute more towards the L-carnitine binding affinity than toward the studied PFASs. For the dimer pocket, the binding affinity of L-carnitine is one of the largest binding energies. The high affinity of L-carnitine to both pockets demonstrates that it could viably be used to compete/replace PFASs from the binding sites. The important interactions detailed here can provide useful insights about how these species may interact with other proteins and about traits that may be important in building an inhibitor that can help to alleviate the effects of these "forever chemicals" on PPARγ.

■ ASSOCIATED CONTENT

Supporting Information

The Supporting Information is available free of charge at https://pubs.acs.org/doi/10.1021/acsomega.1c01304.

PFASs used in this study, PFAS chemical structures used in this study, binding energies for the dimer pocket, binding energies for the LBP, binding poses of PFAS and L-carnitine on PPARγ dimer pocket, average binding energies of PFASs and L-carnitine on the dimer pocket, comparison of MMGBSA results for the LBP with experimental IC_{50} values, binding contribution of each nearby residue for PFASs and L-carnitine (dimer pocket), binding contributions of the acidic and basic residues for PFASs (dimer pocket) in chain A and chain B, binding contributions of the acidic and basic residues for L-carnitine (dimer pocket) in chain A and chain B, hydrogen bond lifetimes for the dimer pocket, PFOS rmsd plots for the dimer pocket, L-carnitine rmsd plots for the dimer pocket, PFOS rmsd plots for the LBP pocket, and L-carnitine rmsd plots for the LBP pocket (PDF)

■ AUTHOR INFORMATION

Corresponding Author

Angela K. Wilson − *Department of Chemistry, Michigan State University, East Lansing, Michigan 48864, United States;* orcid.org/0000-0001-9500-1628; Email: akwilson@msu.edu

Authors

Nuno M. S. Almeida − *Department of Chemistry, Michigan State University, East Lansing, Michigan 48864, United States;* orcid.org/0000-0002-6091-7289

Yiğitcan Eken − *Department of Chemistry, Michigan State University, East Lansing, Michigan 48864, United States;* orcid.org/0000-0002-1762-5790

Complete contact information is available at: https://pubs.acs.org/10.1021/acsomega.1c01304

Notes

The authors declare no competing financial interest.

■ ACKNOWLEDGMENTS

We gratefully acknowledge support from the University of North Texas Academic Computing Services for the use of the UNT Research Clusters and Institute for Cyber-Enabled Research (iCER) at Michigan State University. Computational resources were provided *via* the NSF Major Research Instrumentation program supported by the National Science Foundation under grant no. CHE-1531468.

■ REFERENCES

(1) Sinclair, G. M.; Long, S. M.; Jones, O. A. H. What Are the Effects of PFAS Exposure at Environmentally Relevant Concentrations? *Chemosphere* **2020**, *258*, 127340.
(2) Paul, A. G.; Jones, K. C.; Sweetman, A. J. A First Global Production, Emission, and Environmental Inventory for Perfluorooctane Sulfonate. *Environ. Sci. Technol.* **2009**, *43*, 386−392.
(3) Sajid, M.; Ilyas, M. PTFE-Coated Non-Stick Cookware and Toxicity Concerns: A Perspective. *Environ. Sci. Pollut. Res.* **2017**, *24*, 23436−23440.
(4) Rao, N. S.; Baker, B. E. Textile Finishes and Fluorosurfactants. In *Organofluorine Chemistry*; Banks, R. E., Smart, B. E., Tatlow, J. C., Eds.; Springer US: Boston, MA, 1994, pp 321−338.
(5) Schaider, L. A.; Balan, S. A.; Blum, A.; Andrews, D. Q.; Strynar, M. J.; Dickinson, M. E.; Lunderberg, D. M.; Lang, J. R.; Peaslee, G. F. Fluorinated Compounds in U.S. Fast Food Packaging. *Environ. Sci. Technol. Lett.* **2017**, *4*, 105−111.
(6) State of Minnesota. Civil Action No. 27-CV-10-28862, State of Minnesota, et al. v. 3M Company. Expert Report of Philippe Grandjean, MD, DMSc. Prepared on Behalf of Plaintiff State of Minnesota; State of Minnesota District Court for the County of Hennepin; 2017.
(7) US EPA EPA and 3M announce phase out of PFOS. https://archive.epa.gov/epapages/newsroom_archive/newsreleases/33aa946e6cb11f35852568e1005246b4.html (accessed 2021-06-02).
(8) Wang, Z.; Dewitt, J. C.; Higgins, C. P.; Cousins, I. T. A Never-Ending Story of Per- and Polyfluoroalkyl Substances (PFASs)? *Environ. Sci. Technol.* **2017**, *51*, 2508−2518.
(9) Post, G. B.; Gleason, J. A.; Cooper, K. R. Key Scientific Issues in Developing Drinking Water Guidelines for Perfluoroalkyl Acids: Contaminants of Emerging Concern. *PLoS Biol.* **2017**, *15*, No. e2002855.
(10) Cordner, A.; De La Rosa, V. Y.; Schaider, L. A.; Rudel, R. A.; Richter, L.; Brown, P. Guideline Levels for PFOA and PFOS in Drinking Water: The Role of Scientific Uncertainty, Risk Assessment Decisions, and Social Factors. *J. Expo. Sci. Environ. Epidemiol.* **2019**, *29*, 157−171.
(11) Zeng, Z.; Song, B.; Xiao, R.; Zeng, G.; Gong, J.; Chen, M.; Xu, P.; Zhang, P.; Shen, M.; Yi, H. Assessing the Human Health Risks of Perfluorooctane Sulfonate by in Vivo and in Vitro Studies. *Environ. Int.* **2019**, *126*, 598−610.
(12) Takacs, M. L.; Abbott, B. D. Activation of Mouse and Human Peroxisome Proliferator-Activated Receptors (α, β/δ, γ) by Perfluorooctanoic Acid and Perfluorooctane Sulfonate. *Toxicol. Sci.* **2007**, *95*, 108−117.
(13) Ikeda, T.; Aiba, K.; Fukuda, K.; Tanaka, M. The Induction of Peroxisome Proliferation in Rat Liver by Perfluorinated Fatty Acids, Metabolically Inert Derivatives of Fatty Acids. *J. Biochem.* **1985**, *98*, 475−482.
(14) Butenhoff, J. L.; Pieterman, E.; Ehresman, D. J.; Gorman, G. S.; Olsen, G. W.; Chang, S.-C.; Princen, H. M. G. Distribution of Perfluorooctanesulfonate and Perfluorooctanoate into Human Plasma Lipoprotein Fractions. *Toxicol. Lett.* **2012**, *210*, 360−365.
(15) MacManus-Spencer, L. A.; Tse, M. L.; Hebert, P. C.; Bischel, H. N.; Luthy, R. G. Binding of Perfluorocarboxylates to Serum Albumin: A Comparison of Analytical Methods. *Anal. Chem.* **2010**, *82*, 974−981.
(16) Zhang, X.; Chen, L.; Fei, X.-C.; Ma, Y.-S.; Gao, H.-W. Binding of PFOS to Serum Albumin and DNA: Insight into the Molecular Toxicity of Perfluorochemicals. *BMC Mol. Biol.* **2009**, *10*, 16.
(17) Zhang, L.; Ren, X.-M.; Wan, B.; Guo, L.-H. Structure-Dependent Binding and Activation of Perfluorinated Compounds on Human Peroxisome Proliferator-Activated Receptor γ. *Toxicol. Appl. Pharmacol.* **2014**, *279*, 275−283.
(18) Behr, A.-C.; Plinsch, C.; Braeuning, A.; Buhrke, T. Activation of Human Nuclear Receptors by Perfluoroalkylated Substances (PFAS). *Toxicol. Vitro* **2020**, *62*, 104700.
(19) Pastoor, T. P.; Lee, K. P.; Perri, M. A.; Gillies, P. J. Biochemical and Morphological Studies of Ammonium Perfluorooctanoate-Induced Hepatomegaly and Peroxisome Proliferation. *Exp. Mol. Pathol.* **1987**, *47*, 98−109.
(20) Abdellatif, A.; Préat, V.; Taper, H. S.; Roberfroid, M. The Modulation of Rat Liver Carcinogenesis by Perfluorooctanoic Acid, a Peroxisome Proliferator. *Toxicol. Appl. Pharmacol.* **1991**, *111*, 530−537.
(21) Ren, X.-M.; Qin, W.-P.; Cao, L.-Y.; Zhang, J.; Yang, Y.; Wan, B.; Guo, L.-H. Binding Interactions of Perfluoroalkyl Substances with Thyroid Hormone Transport Proteins and Potential Toxicological Implications. *Toxicology* **2016**, *366-367*, 32−42.
(22) Zhang, L.; Ren, X.-M.; Guo, L.-H. Structure-Based Investigation on the Interaction of Perfluorinated Compounds with Human Liver Fatty Acid Binding Protein. *Environ. Sci. Technol.* **2013**, *47*, 11293−11301.
(23) Han, X.; Snow, T. A.; Kemper, R. A.; Jepson, G. W. Binding of Perfluorooctanoic Acid to Rat and Human Plasma Proteins. *Chem. Res. Toxicol.* **2003**, *16*, 775−781.
(24) Wang, Y.; Zhang, H.; Kang, Y.; Cao, J. Effects of Perfluorooctane Sulfonate on the Conformation and Activity of Bovine Serum Albumin. *J. Photochem. Photobiol., B* **2016**, *159*, 66−73.
(25) Beesoon, S.; Martin, J. W. Isomer-Specific Binding Affinity of Perfluorooctanesulfonate (PFOS) and Perfluorooctanoate (PFOA) to Serum Proteins. *Environ. Sci. Technol.* **2015**, *49*, 5722−5731.
(26) Honda, M.; Muta, A.; Akasaka, T.; Inoue, Y.; Shimasaki, Y.; Kannan, K.; Okino, N.; Oshima, Y. Identification of Perfluorooctane Sulfonate Binding Protein in the Plasma of Tiger Pufferfish Takifugu Rubripes. *Ecotoxicol. Environ. Saf.* **2014**, *104*, 409−413.
(27) Chou, H.-C.; Wen, L.-L.; Chang, C.-C.; Lin, C.-Y.; Jin, L.; Juan, S.-H. L-Carnitine via PPARγ- and Sirt1-Dependent Mechanisms Attenuates Epithelial-Mesenchymal Transition and Renal Fibrosis Caused by Perfluorooctanesulfonate. *Toxicol. Sci.* **2017**, *160*, 217−229.
(28) Wen, L.-L.; Lin, C.-Y.; Chou, H.-C.; Chang, C.-C.; Lo, H.-Y.; Juan, S.-H. Perfluorooctanesulfonate Mediates Renal Tubular Cell Apoptosis through PPARgamma Inactivation. *PLoS One* **2016**, *11*, No. e0155190.
(29) Liu, W.-S.; Lai, Y.-T.; Chan, H.-L.; Li, S.-Y.; Lin, C.-C.; Liu, C.-K.; Tsou, H.-H.; Liu, T.-Y. Associations between Perfluorinated Chemicals and Serum Biochemical Markers and Performance Status in Uremic Patients under Hemodialysis. *PLoS One* **2018**, *13*, No. e0200271.
(30) Fulton, J.; Mazumder, B.; Whitchurch, J. B.; Monteiro, C. J.; Collins, H. M.; Chan, C. M.; Clemente, M. P.; Hernandez-Quiles, M.; Stewart, E. A.; Amoaku, W. M.; et al. Heterodimers of Photoreceptor-Specific Nuclear Receptor (PNR/NR2E3) and Peroxisome Proliferator-Activated Receptor-γ (PPARγ) Are Disrupted by Retinal Disease-Associated Mutations. *Cell Death Dis.* **2017**, *8*, No. e2677.
(31) Todorov, V. T.; Desch, M.; Schmitt-Nilson, N.; Todorova, A.; Kurtz, A. Peroxisome Proliferator-Activated Receptor-γ Is Involved in the Control of Renin Gene Expression. *Hypertension* **2007**, *50*, 939−944.
(32) Estany, J.; Ros-Freixedes, R.; Tor, M.; Pena, R. N. A Functional Variant in the Stearoyl-CoA Desaturase Gene Promoter Enhances Fatty Acid Desaturation in Pork. *PLoS One* **2014**, *9*, No. e86177.
(33) Okuno, M.; Arimoto, E.; Ikenobu, Y.; Nishihara, T.; Imagawa, M. Dual DNA-Binding Specificity of Peroxisome-Proliferator-

Activated Receptor γ Controlled by Heterodimer Formation with Retinoid X Receptor α. *Biochem. J.* **2001**, *353*, 193−198.
(34) Nolte, R. T.; Wisely, G. B.; Westin, S.; Cobb, J. E.; Lambert, M. H.; Kurokawa, R.; Rosenfeld, M. G.; Willson, T. M.; Glass, C. K.; Milburn, M. V. Ligand Binding and Co-Activator Assembly of the Peroxisome Proliferator-Activated Receptor-γ. *Nature* **1998**, *395*, 137−143.
(35) Waku, T.; Shiraki, T.; Oyama, T.; Maebara, K.; Nakamori, R.; Morikawa, K. The Nuclear Receptor PPARγ Individually Responds to Serotonin-and Fatty Acid-Metabolites. *EMBO J.* **2010**, *29*, 3395−3407.
(36) Salvalaglio, M.; Muscionico, I.; Cavallotti, C. Determination of Energies and Sites of Binding of PFOA and PFOS to Human Serum Albumin. *J. Phys. Chem. B* **2010**, *114*, 14860−14874.
(37) Ng, C. A.; Hungerbuehler, K. Exploring the Use of Molecular Docking to Identify Bioaccumulative Perfluorinated Alkyl Acids (PFAAs). *Environ. Sci. Technol.* **2015**, *49*, 12306−12314.
(38) Chen, H.; He, P.; Rao, H.; Wang, F.; Liu, H.; Yao, J. Systematic Investigation of the Toxic Mechanism of PFOA and PFOS on Bovine Serum Albumin by Spectroscopic and Molecular Modeling. *Chemosphere* **2015**, *129*, 217−224.
(39) Zhang, W.; Xiong, X.; Wang, F.; Ge, Y.; Liu, Y. Studies of the Interaction between Ronidazole and Human Serum Albumin by Spectroscopic and Molecular Docking Methods. *J. Solution Chem.* **2013**, *42*, 1194−1206.
(40) Cheng, W.; Ng, C. A. Predicting Relative Protein Affinity of Novel Per- and Polyfluoroalkyl Substances (PFASs) by An Efficient Molecular Dynamics Approach. *Environ. Sci. Technol.* **2018**, *52*, 7972−7980.
(41) Tsukahara, T.; Tsukahara, R.; Yasuda, S.; Makarova, N.; Valentine, W. J.; Allison, P.; Yuan, H.; Baker, D. L.; Li, Z.; Bittman, R.; et al. Different Residues Mediate Recognition of 1-O-Oleyl-Lysophosphatidic Acid and Rosiglitazone in the Ligand Binding Domain of Peroxisome Proliferator-Activated Receptor. *J. Biol. Chem.* **2006**, *281*, 3398−3407.
(42) Uppenberg, J.; Svensson, C.; Jaki, M.; Bertilsson, G.; Jendeberg, L.; Berkenstam, A. Crystal Structure of the Ligand Binding Domain of the Human Nuclear Receptor PPARgamma. *J. Biol. Chem.* **1998**, *273*, 31108−31112.
(43) Zoete, V.; Grosdidier, A.; Michielin, O. Peroxisome Proliferator-Activated Receptor Structures: Ligand Specificity, Molecular Switch and Interactions with Regulators. *Biochim. Biophys. Acta Mol. Cell Biol. Lipids* **2007**, *1771*, 915−925.
(44) Li, C.-H.; Ren, X.-M.; Cao, L.-Y.; Qin, W.-P.; Guo, L.-H. Investigation of Binding and Activity of Perfluoroalkyl Substances to the Human Peroxisome Proliferator-Activated Receptor β/δ. *Environ. Sci.: Processes Impacts* **2019**, *21*, 1908−1914.
(45) Wang, Z.; Cousins, I. T.; Scheringer, M.; Hungerbühler, K. Fluorinated Alternatives to Long-Chain Perfluoroalkyl Carboxylic Acids (PFCAs), Perfluoroalkane Sulfonic Acids (PFSAs) and Their Potential Precursors. *Environ. Int.* **2013**, *60*, 242−248.
(46) Poulsen, P. B.; Jensen, A. A.; Wallström, E.; Aps, E. *More Environmentally Friendly Alternatives to PFOS-Compounds and PFOA*, 2005.report
(47) Wang, Y.; Chang, W.; Wang, L.; Zhang, Y.; Zhang, Y.; Wang, M.; Wang, Y.; Li, P. A Review of Sources, Multimedia Distribution and Health Risks of Novel Fluorinated Alternatives. *Ecotoxicol. Environ. Saf.* **2019**, *182*, 109402.
(48) Labute, P. Protonate3D: Assignment of Ionization States and Hydrogen Coordinates to Macromolecular Structures. *Proteins: Struct., Funct., Bioinf.* **2009**, *75*, 187−205.
(49) *Molecular Operating Environment (MOE)*; Chemical Computing Group Inc.: Montreal, Canada, 2016.
(50) Labute, P.; Santavy, M. SiteFinder-Locating Binding Sites in Protein Structures. http://www.chemcomp.com (accessed 2020-06-02).
(51) Kim, S.; Chen, J.; Cheng, T.; Gindulyte, A.; He, J.; He, S.; Li, Q.; Shoemaker, B. A.; Thiessen, P. A.; Yu, B.; et al. PubChem 2019 Update: Improved Access to Chemical Data. *Nucleic Acids Res.* **2019**, *47*, D1102−D1109.
(52) Hoffmann, R. An Extended Hückel Theory. I. Hydrocarbons. *J. Chem. Phys.* **1963**, *39*, 1397−1412.
(53) Hornak, V.; Abel, R.; Okur, A.; Strockbine, B.; Roitberg, A.; Simmerling, C. Comparison of Multiple Amber Force Fields and Development of Improved Protein Backbone Parameters. *Proteins Struct. Funct. Genet.* **2006**, *65*, 712−725.
(54) Wang, J.; Wolf, R. M.; Caldwell, J. W.; Kollman, P. A.; Case, D. A. Development and Testing of a General Amber Force Field. *J. Comput. Chem.* **2004**, *25*, 1157−1174.
(55) Corbeil, C. R.; Williams, C. I.; Labute, P. Variability in Docking Success Rates Due to Dataset Preparation. *J. Comput. Aided Mol. Des.* **2012**, *26*, 775−786.
(56) Case, D. A.; Cerutti, D. S.; Cheatham, T. E.; Darden, T. A., III; Duke, R. E.; Giese, T. J.; Gohlke, H.; Goetz, A. W.; Greene, N.; Homeyer, S.; Izadi, A.; Kovalenko, T. S.; Lee, S.; LeGrand, P.; Li, C.; Lin, J.; Liu, T.; Luchko, R. L.; Mermelstein, D.; Merz, K. M.; Monard, G.; Nguyen, H.; Omelyan, I.; Onufriev, A.; Pan, F.; Qi, R.; Roe, D. R.; Roitberg, C.; Sagui, C. L.; Simmerling, W. M.; Botello-Smith, J.; Swails, R. C.; Walker, J.; Wang, R. M.; Wolf, X.; Wu, L.; Xiao, D. M. Y. *Amber17*, 2017.
(57) Maier, J. A.; Martinez, C.; Kasavajhala, K.; Wickstrom, L.; Hauser, K. E.; Simmerling, C. Ff14SB: Improving the Accuracy of Protein Side Chain and Backbone Parameters from Ff99SB. *J. Chem. Theory Comput.* **2015**, *11*, 3696−3713.
(58) Jakalian, A.; Jack, D. B.; Bayly, C. I. Fast, Efficient Generation of High-Quality Atomic Charges. AM1-BCC Model: II. Parameterization and Validation. *J. Comput. Chem.* **2002**, *23*, 1623−1641.
(59) Joung, I. S.; Cheatham, T. E. Determination of Alkali and Halide Monovalent Ion Parameters for Use in Explicitly Solvated Biomolecular Simulations. *J. Phys. Chem. B* **2008**, *112*, 9020−9041.
(60) Ryckaert, J.-P.; Ciccotti, G.; Berendsen, H. J. C. Numerical Integration of the Cartesian Equations of Motion of a System with Constraints: Molecular Dynamics of n-Alkanes. *J. Comput. Phys.* **1977**, *23*, 327−341.
(61) Onufriev, A.; Bashford, D.; Case, D. A. Exploring Protein Native States and Large-Scale Conformational Changes with a Modified Generalized Born Model. *Proteins Struct. Funct. Genet.* **2004**, *55*, 383−394.
(62) Miller, B. R.; McGee, T. D.; Swails, J. M.; Homeyer, N.; Gohlke, H.; Roitberg, A. E. MMPBSA.Py: An Efficient Program for End-State Free Energy Calculations. *J. Chem. Theory Comput.* **2012**, *8*, 3314−3321.
(63) Hou, T.; Wang, J.; Li, Y.; Wang, W. Assessing the Performance of the MM/PBSA and MM/GBSA Methods. 1. The Accuracy of Binding Free Energy Calculations Based on Molecular Dynamics Simulations. *J. Chem. Inf. Model.* **2011**, *51*, 69−82.
(64) Roe, D. R. Introduction to hydrogen bond analysis. https://amber.utah.edu/AMBER-workshop/London-2015/Hbond/ (accessed 2019-04-19).
(65) Liberato, M. V.; Nascimento, A. S.; Ayers, S. D.; Lin, J. Z.; Cvoro, A.; Silveira, R. L.; Martínez, L.; Souza, P. C. T.; Saidemberg, D.; Deng, T.; et al. Medium Chain Fatty Acids Are Selective Peroxisome Proliferator Activated Receptor (PPAR) γ Activators and Pan-PPAR Partial Agonists. *PLoS One* **2012**, *7*, No. e36297.
(66) Shi, G. Q.; Dropinski, J. F.; McKeever, B. M.; Xu, S.; Becker, J. W.; Berger, J. P.; MacNaul, K. L.; Elbrecht, A.; Zhou, G.; Doebber, T. W.; et al. Design and Synthesis of α-Aryloxyphenylacetic Acid Derivatives: A Novel Class of PPARα/γ Dual Agonists with Potent Antihyperglycemic and Lipid Modulating Activity. *J. Med. Chem.* **2005**, *48*, 4457−4468.
(67) Kuwabara, N.; Oyama, T.; Tomioka, D.; Ohashi, M.; Yanagisawa, J.; Shimizu, T.; Miyachi, H. Peroxisome Proliferator-Activated Receptors (PPARs) Have Multiple Binding Points That Accommodate Ligands in Various Conformations: Phenylpropanoic Acid-Type PPAR Ligands Bind to PPAR in Different Conformations, Depending on the Subtype. *J. Med. Chem.* **2012**, *55*, 893−902.

https://doi.org/10.1021/acsomega.1c01304
ACS Omega 2021, 6, 15103−15114

(68) Hughes, T. S.; Giri, P. K.; de Vera, I. M. S.; Marciano, D. P.; Kuruvilla, D. S.; Shin, Y.; Blayo, A.-L.; Kamenecka, T. M.; Burris, T. P.; Griffin, P. R.; et al. An Alternate Binding Site for PPARγ Ligands. *Nat. Commun.* **2014**, *5*, 3571.
(69) Lai, T. T.; Eken, Y.; Wilson, A. K. Binding of Per- and Polyfluoroalkyl Substances to the Human Pregnane X Receptor. *Environ. Sci. Technol.* **2020**, *54*, 15986−15995.
(70) Genheden, S.; Ryde, U. The MM/PBSA and MM/GBSA Methods to Estimate Ligand-Binding Affinities. *Expet Opin. Drug Discov.* **2015**, *10*, 449−461.

https://doi.org/10.1021/acsomega.1c01304
ACS Omega 2021, 6, 15103−15114